THE JOURNAL OF BIOLOGICAL CHEMISTRY VOL. 281, NO. 2, pp. 1296–1304, January 13, 2006

Caspases Target Only Two Architectural Components within the Core Structure of the Nuclear Pore Complex*[S]

Received for publication, October 31, 2005, and in revised form, November 14, 2005 Published, JBC Papers in Press, November 14, 2005, DOI 10.1074/jbc.M511717200

Monika Patre[‡], Anja Tabbert[‡], Daniela Hermann[‡], Henning Walczak[§], Hans-Richard Rackwitz[¶], Volker C. Cordes[‖], and Elisa Ferrando-May[‡1]**

*From the [‡]Molecular Toxicology Group, Faculty of Biology, University of Konstanz, D-78457 Konstanz, Germany, the [§]Tumor Immunology Program Division of Apoptosis Regulation, German Cancer Research Center, INF 280, D-69120 Heidelberg, Germany, the [¶]Peptide Specialty Laboratories GmbH, Sitzbuchweg 12, D-69118 Heidelberg, Germany, the [‖]Department of Cell and Molecular Biology, Karolinska Institutet, S-17177 Stockholm, Sweden, and the **Zentrum fuer Molekulare Biologie Heidelberg, University of Heidelberg, INF 282, D-69120 Heidelberg, Germany*

Caspases were recently implicated in the functional impairment of the nuclear pore complex during apoptosis, affecting its dual activity as nucleocytoplasmic transport channel and permeability barrier. Concurrently, electron microscopic data indicated that nuclear pore morphology is not overtly altered in apoptotic cells, raising the question of how caspases may deactivate nuclear pore function while leaving its overall structure largely intact. To clarify this issue we have analyzed the fate of all known nuclear pore proteins during apoptotic cell death. Our results show that only two of more than 20 nuclear pore core structure components, namely Nup93 and Nup96, are caspase targets. Both proteins are cleaved near their N terminus, disrupting the domains required for interaction with other nucleoporins actively involved in transport and providing the permeability barrier but dispensable for maintaining the nuclear pore scaffold. Caspase-mediated proteolysis of only few nuclear pore complex components may exemplify a general strategy of apoptotic cells to efficiently disable huge macromolecular machines.

Caspases are a family of highly specific cysteine proteases that play a central role in programmed cell death by apoptosis (1). By cleavage of a limited number of structural and regulatory proteins, they produce changes in cellular morphology and metabolism that are hallmarks of the apoptotic process. In the nucleus such changes include pronounced chromatin condensation, massive nucleosomal DNA fragmentation, and alterations in nuclear shape (2, 3). Recent reports also indicate that the regulated exchange of macromolecules between the nucleus and cytoplasm is impaired during apoptosis (4–8).

Regulated nucleocytoplasmic transport across the nuclear envelope occurs via nuclear pore complexes (NPCs),[2] channels of elaborate architecture that consist of multiple copies of about 30 different nucleoporins (9). Many nucleoporins are components of distinct subcomplexes that are arranged around the central pore channel in 8-fold rotational symmetry. The vertebrate Nup93 subcomplex, embedded within the NPC core, harbors Nup205, Nup188, and Nup93 (10–12). This subcomplex is believed to be an anchor site for the Nup62 subcomplex that resides close to the pore channel mid-axis and consists of Nup62, Nup58, and Nup54 (13, 14). The Nup93 subcomplex furthermore is flanked on both sides by the Nup160 subcomplex, consisting of nine proteins, *i.e.* Nup160, Nup133, Nup107, Nup96, Nup75/85, Nup43, Nup37, Sec13, and Seh1 (12, 15–18). Another nucleoporin, Nup98 (19, 20), is not stably integrated in the Nup160 subcomplex but interacts with one of its components, Nup96 (16, 21). Whether other NPC core components, namely Nup155 (22), NLP1/CG1 (23), Nup35, and Aladin (9) directly interact with any known subcomplex or might be part of yet another still needs to be investigated.

These subcomplexes are thought to be anchored to the pore wall by direct or indirect interaction with transmembrane proteins. Two such pore wall transmembrane proteins, gp210 (24, 25) and Pom121 (26), have been identified in higher eukaryotes to date, but their potential role as anchoring proteins still needs clarification.

In addition to these components of the central NPC core framework, eight fibrils of distinctive shape and composition are built upon each side of the NPC. Fibers on the cytoplasmic face consist of RanBP2/Nup358 (27, 28). NPC attachment of RanBP2 is mediated by Nup214 (29, 30) and Nup88 (31–33), all of which are exclusively cytoplasmic nucleoporins. The fibrils emanating from the nucleoplasmic side of the NPC are longer and interconnected at their distal ends, forming a structure called the nuclear basket (34, 35). Tpr, a coiled-coil protein of 267 kDa (36), is believed to be the central architectural component of the basket (12). NPC attachment of Tpr is mediated by Nup153, a predominantly nuclear protein (37–39) that also represents a binding site for Nup50, a mobile nucleoporin located both within the nuclear interior and at the NPC (40, 41). Nup153 in turn binds to the NPC by direct interaction with the Nup160 subcomplex (16).

Several nucleoporins contain domains characterized by phenylalanine-glycine (FG) repeats separated by polar spacer sequences (42). Vectorial movement across the NPC requires direct interaction between the translocating molecules and these FG repeat regions (43). At the same time, FG repeats have been proposed to form a meshwork within the pore channel that acts as the permeability barrier for macromolecules that need to be retained either in the nucleus or the cytoplasm (44). In mammals, the FG repeat nucleoporins comprise Nup62, Nup58, Nup54, NLP1/CG1, Pom121, RanBP2/Nup358, Nup214, Nup153, and Nup98.

So far, seven nucleoporins have been investigated in cells undergoing apoptosis, including the peripheral RanBP2, Nup214, Nup153, and Tpr, the transmembrane proteins Pom121 and gp120, and the NPC core

* This work was supported by grants from the Swedish Natural Research Council (to V. C. C.) and Deutsche Forschungsgemeinschaft Grant FOR 324/2-2 (to E. F.-M.). The costs of publication of this article were defrayed in part by the payment of page charges. This article must therefore be hereby marked "*advertisement*" in accordance with 18 U.S.C. Section 1734 solely to indicate this fact.

[S] The on-line version of this article (available at http://www.jbc.org) contains supplemental Fig. S1 and supplemental Table S2.

[1] To whom correspondence should be addressed: University of Konstanz, P.O. Box X911, D-78457 Konstanz, Germany. Tel.: 49-7531-884054; Fax: 49-7531-884033; E-mail: elisa.may@uni-konstanz.de.

[2] The abbreviations used are: NPC, nuclear pore complex; FG, phenylalanine-glycine; TRAIL, tumor necrosis factor-related apoptosis-inducing ligand; FACS, fluorescence-activated cell sorter; PBS, phosphate-buffered saline; CHAPS, 3-[(3-cholamidopropyl)dimethylammonio]-1-propanesulfonic acid; aa, amino acid(s).

component Nup62. Of these, only Nup62 and gp120 were found not degraded, whereas the other five proteins were described as targets for caspase-mediated proteolysis (5, 7, 45). The overall morphology of such apoptotic NPCs appears strikingly preserved in electron microscopic images, suggesting that other core nucleoporins, in addition to Nup62 and gp210, might be spared by caspases and thus keep up an NPC scaffold (45–47). However, it was also shown that the ability of the NPC to act as a permeability barrier for certain macromolecules and to sustain nucleocytoplasmic transport of others is compromised during apoptosis (4–6, 8). These observations cannot be explained exclusively by cleavage of peripheral nucleoporins, indicating that in fact some NPC core components might also be altered in the course of cell death.

Because of the limited number of nucleoporins analyzed so far, it has not been possible yet to correlate the data regarding morphology and function of the apoptotic NPC on the one hand to the preservation or loss of individual nucleoporins on the other. The recent progress in the elucidation of NPC protein composition and the availability of increasing numbers of nucleoporin-specific antibodies have therefore prompted us to study the fate of all NPC components during apoptosis. To also clarify how different cell death signaling cascades might affect individual nucleoporins, we used two apoptosis model systems in which cells are exposed to drugs that initiate the apoptotic response on either the one or other side of the nuclear envelope.

In the first model, apoptosis was triggered at the plasma membrane by stimulation with the tumor necrosis factor-related apoptosis-inducing ligand (TRAIL), which induces apoptosis by binding to two death-domain containing TRAIL receptors (48, 49). As an apoptotic insult directed to the nucleus we chose etoposide, an inhibitor of type II DNA topoisomerases. Treatment with etoposide results in the accumulation of DNA double-stranded breaks that act as potent apoptotic triggers (50).

Our results indicate that except for Nup93 and Nup96, which are processed in both models at the onset of the apoptotic execution phase, the NPC core structure is not subject to caspase-mediated degradation. Conversely, most nucleoporins that are peripherally attached to the cytoplasmic and nuclear side of the NPC are favored caspase substrates, although they respond differently to the different apoptotic stimuli with respect to the timing and extent of their degradation. These data provide a comprehensive analysis of the apoptotic fate of a supramolecular assembly, illustrating how the apoptotic machinery may proceed in shutting down crucial cellular functions by targeting strategic sites within complex multimeric structures.

EXPERIMENTAL PROCEDURES

Cell Culture and Induction of Apoptosis—HeLa 229 cells were grown in Dulbecco's modified Eagle's medium with 10% fetal calf serum. For induction of apoptosis, lz-TRAIL (51) and etoposide (Sigma) were added to final concentrations of 300 ng/ml and 50 μM, respectively. For protease inhibitor assays, the cells were preincubated with inhibitors 30 min before induction (20 μM for all inhibitors except CA-074-Me (100 μM); all from Bachem Biochemica). For synchronization in cell cycle G_1 phase, the cells were incubated in medium with 2.2 mM thymidine for 12 h. After washings and incubation in fresh medium for 9 h, the cells were treated once more with 2.2 mM thymidine for 12 h. Apoptosis was induced by etoposide or TRAIL 4 h after release from the second metabolic block.

FACS Analysis—HeLa 229 cells were collected by gently scraping them off the culture dish in ice-cold PBS. Following washes and resuspension in ice-cold PBS, the cells were fixed by dropwise addition of a 4-fold excess of ice-cold ethanol under gentle stirring and stored overnight at 4 °C. The cells were then collected by centrifugation and resuspended in PBS containing 100 μg/ml RNase A. After the addition of 40 μg/ml propidium iodide, the cells were analyzed by FACS in a Becton Dickinson LSR flow cytometer. At least 1×10^4 cells were sorted per FACS experiment. The measurements were repeated three times.

Quantification of Apoptosis by Scoring Condensed Nuclei—HeLa cell cultures were stained with a mixture of the membrane-permeable DNA dye H-33342 (500 ng/ml; Molecular Probes) and the membrane-impermeable DNA dye SYTOX (500 nM; Molecular Probes). Cells with intact plasma membrane and characteristically condensed or fragmented nuclei were scored as apoptotic. The data were collected from a minimum of three independent experiments.

Quantification of Oligonucleosomal DNA Fragmentation—The production of histone-associated DNA fragments (mono- and oligonucleosomes) was assessed with the cell death detection enzyme-linked immunosorbent assay (Roche Applied Science) according to the instructions of the manufacturer. Briefly, the cells were lysed, and the cytoplasmic fraction was recovered by centrifugation. Nucleosomal concentration in this fraction was determined by a sandwich enzyme-linked immunosorbent assay, using histone-specific antibodies preadsorbed to microtiter plates and peroxidase-conjugated antibodies against DNA. Peroxidase activity was measured photometrically. The experiments were run in triplicate.

Measurement of Caspase Activity—Caspase-3-like activity was measured as the degree of DEVD-afc (*N*-acetyl-Asp-Glu-Val-aspartyl-aminofluoro-methylcoumarine; Bachem Biochemica) cleavage and was assayed essentially as described earlier (52, 53). The cells were lysed in 25 mM HEPES, pH 7.5, 5 mM $MgCl_2$, 1 mM EGTA, 0.5% Triton X-100. The fluorimetric assay was carried out in microtiter plates with a substrate concentration of 40 μM and a total protein amount of 3–4 μg. Cleavage of DEVD-afc was followed in reaction buffer (50 mM HEPES, pH 7.5, 10 mM dithiothreitol, 1% sucrose, 0.1% CHAPS) over a period of 20 min at 37 °C with $\lambda_{ex} = 390$ nm and $\lambda_{em} = 505$ nm. The activity was calibrated with afc standard solutions. The measurements were run in triplicate and repeated at least three times.

Preparation of Whole Cell Extracts—For the preparation of protein extracts, HeLa cell cultures were placed on ice, and protease inhibitors (Complete Mix; Roche Applied Science) and dithiothreitol (1 mM) were added directly to the growth media. The cells were then gently scraped off the dish with a rubber policeman, washed in ice-cold PBS, resuspended in 95 °C lysis buffer (50 mM Tris/HCl, pH 8.0, 0.5% SDS, 1 mM dithiothreitol), and heated at 95 °C for 10 min. The cell debris was removed by centrifugation at 20,000 × *g* for 10 min.

SDS Gel Electrophoresis and Immunoblotting—SDS-PAGE was according to Thomas and Kornberg (54). The proteins were blotted onto nitrocellullose using a wet blot chamber (Bio-Rad Trans-Blot Cell), and the filters were then incubated in TNT buffer (50 mM Tris, pH 8.0, 150 mM NaCl, 0.05% Tween 20) with 5% milk powder at room temperature for 1 h. Incubation with primary antibodies at 4 °C was in TNT with milk overnight. Filter washings were in TNT alone. Incubations with horseradish peroxidase-coupled secondary antibodies were in TNT with milk at room temperature for 1 h. The filter strip with the biotinylated molecular weight marker (Bio-Rad) was incubated separately with horseradish peroxidase-coupled avidin for 30 min at room temperature. Immunoblots were visualized with a chemiluminescent image analyzer (LAS-1000; Fujifilm), and the images were evaluated with the AIDA software package (Fujifilm). The signal intensity was integrated over the signal area and corrected for the background intensity. The percentage of cleavage was calculated as the ratio between the

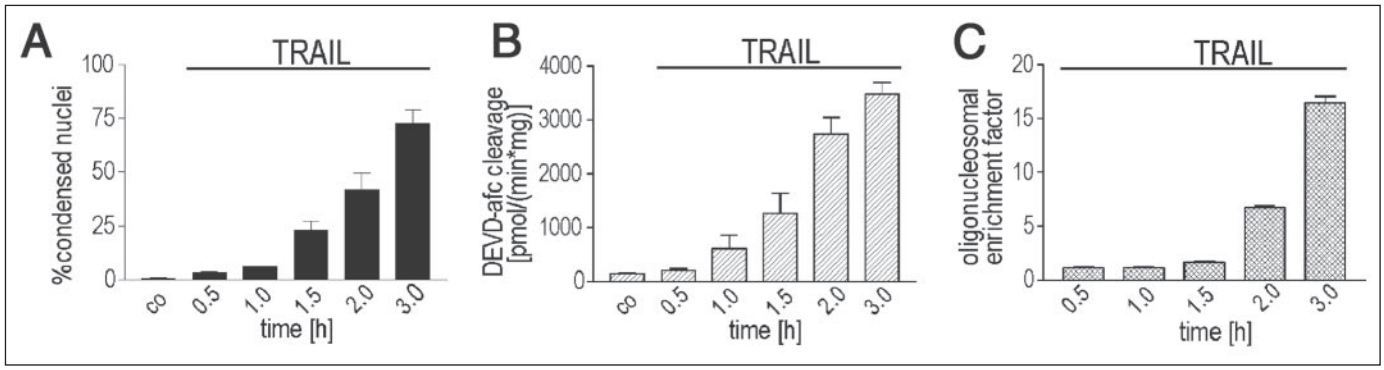

FIGURE 1. **TRAIL-induced apoptosis in HeLa cells.** HeLa cells were treated with 300 ng/ml TRAIL. At indicated time points, apoptosis was assessed by measurement of three different end points. *A*, cells were stained with Hoechst 33342 and inspected microscopically. Cells with condensed nuclei were scored as apoptotic. *B*, caspase 3/7-like activity was determined by fluorimetric detection of DEVD-afc cleavage. *C*, oligonucleosomal DNA fragmentation was quantified by an enzyme-linked immunosorbent assay specific for histone-bound DNA fragments. The bar diagrams indicate increase in oligonucleosome concentration relative to untreated cells. The data are the means ± standard deviation from triplicate determinations.

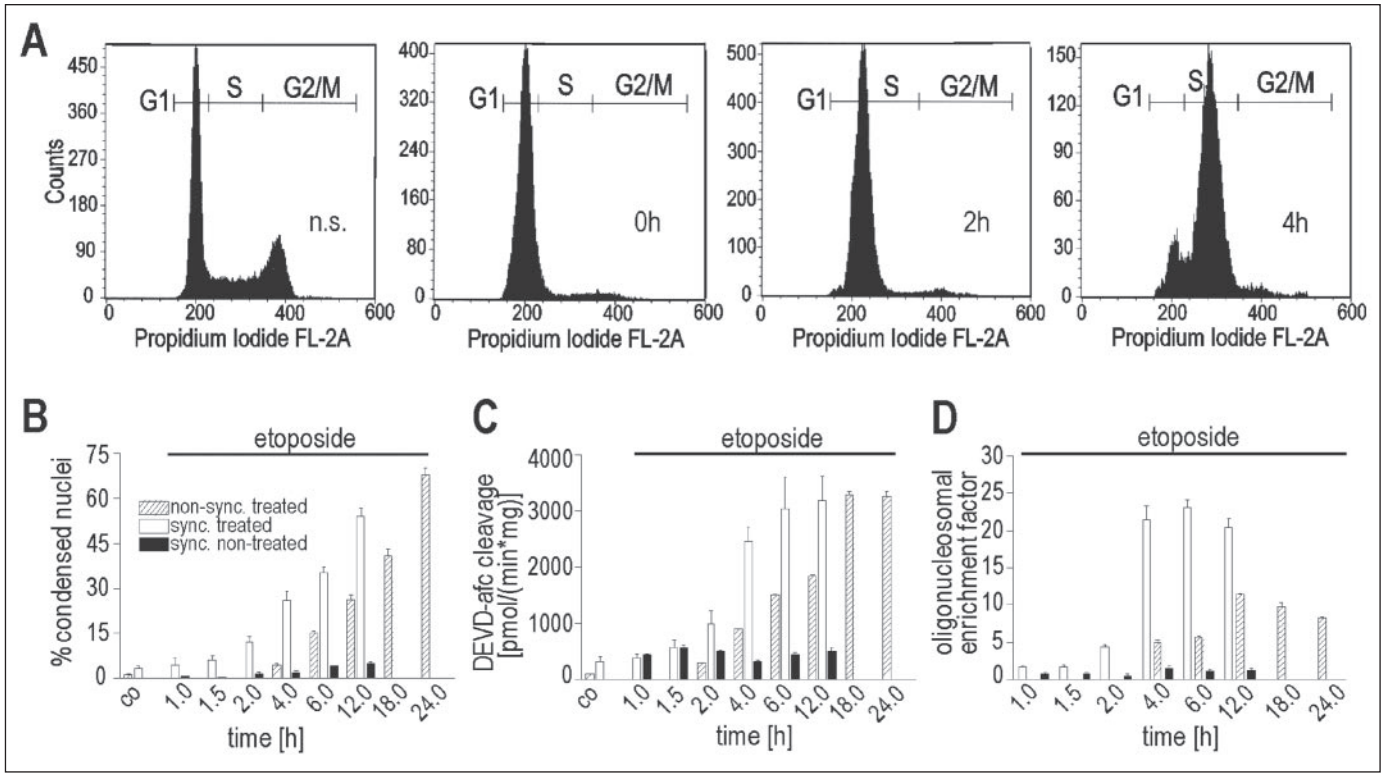

FIGURE 2. **Cell synchronization in the S phase amplifies the apoptosis-inducing effect of etoposide.** *A*, FACS data of a nonsynchronized HeLa cell population (*n.s.*), cells synchronized in G_1/S by a double thymidine block (*0h*), and 2 and 4 h (*2h* and *4h*, respectively) after metabolic block release. *B–D*, 4 h after release from the second block, cells were treated with 50 μM etoposide. At indicated time points, apoptosis was assessed as in Fig. 1. *B*, condensed nuclei. *C*, caspase 3/7-like activity. *D*, oligonucleosomal DNA fragmentation. The data are the means ± standard deviation from triplicate determinations. *Open bars*, synchronized, etoposide-treated cells; *hatched bars*, nonsynchronized, etoposide-treated cells; *black bars*, synchronized, nontreated cells.

integrated signal intensities of the predominant proteolytic products and the intact polypeptides.

Antibodies—Antibodies used in this study are listed in supplemental Table S1; those listed in bold letters have been used for the immunoblots shown in Figs. 4 and 5. Immunization of guinea pigs and rabbits and purification of peptide antibodies was as reported earlier (36, 39). Monoclonal antibody PF190 × 7A8 against Nup153 (55), monoclonal antibody 203-37 against Tpr (36), polyclonal guinea pig antibodies against recombinant Nup62 (56), and peptide antibodies against Nup50, Nup93, Nup96, Nup98, Nup107, Nup205, and RanBP2 (5, 12, 39) have been described earlier. Monoclonal antibodies against Nup88 were from BD Biosciences. Novel rabbit and guinea pig peptide antibodies were raised against Nup35, Nup37, Nup50, Nup54, Nup58, Nup62, Nup155, Nup205, Nup214, Pom121, gp210, Seh1, Aladin, and NLP1/CG1, according to the procedure described before (39). Other antibodies against RanBP2, Nup214, Nup133, Nup107, POM121, and Sec13 and against Nup160, Nup188, and Nup75 were kindly provided by Frauke Melchior, Ralph Kehlenbach, Valerie Doye, Dirk Goerlich, Wanjin Hong, and Jochen Koeser, respectively.

RESULTS

Two Models of Apoptosis for the Study of NPC Proteolysis—For the induction of apoptosis at the plasma membrane, HeLa cells were treated with TRAIL. The time course of apoptosis was characterized by assess-

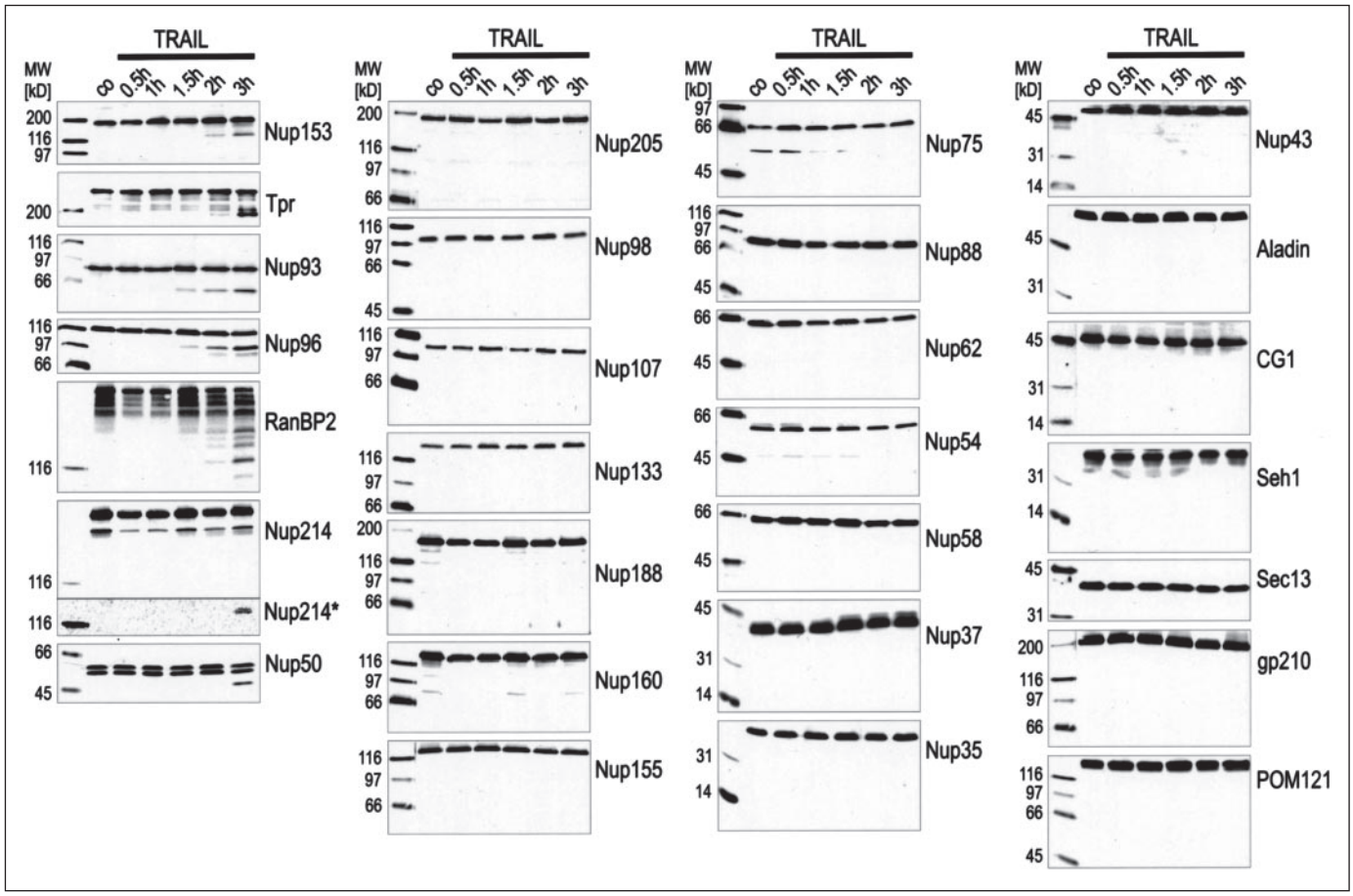

FIGURE 3. **Peripheral nucleoporins and two components of the NPC core structure, Nup93 and Nup96, are cleaved during TRAIL-induced apoptosis.** Whole cell extracts were prepared from control (*co*) and apoptotic HeLa cells treated with 300 ng/ml TRAIL. The cells were collected at the indicated time points, followed by immunoblot analysis with antibodies specific for indicated nucleoporins. A long exposure of the Nup214 immunoblot (*asterisk*) is included.

ing three characteristic end points, namely (i) chromatin condensation, (ii) activation of executor caspases, and (iii) oligonucleosomal DNA fragmentation.

In this model, most cells displayed the typical apoptotic morphology within 3 h after stimulation. This was paralleled by an increase of caspase-3/7-like activity and enrichment of oligonucleosomal DNA fragments (Fig. 1), collectively indicating a highly synchronous onset of the apoptotic execution routine.

For the induction of apoptosis directly within the nucleus, we used etoposide, a well characterized inducer of DNA damage. In contrast to the more rapid response to TRAIL, etoposide-induced apoptosis in HeLa cells has been reported to occur in the time range of 24–48 h (57, 58). This is partly due to the cell cycle dependence of etoposide toxicity, which is highest during the S phase (59). To accelerate the onset of etoposide-induced apoptosis, thereby allowing a more direct comparison between the two models, we first synchronized HeLa cells by a double thymidine block, which arrests the cells at the G_1/S phase transition. After releasing these cells from the second block, most of them synchronously traversed the S phase, as shown by FACS analysis (Fig. 2*A*). Their response to treatment with 50 μM etoposide was then compared with that of a nonsynchronized cell population. 4 h after drug addition, the synchronized population displayed a 5-fold increase in the number of apoptotic cells compared with nonsynchronized cells. This was paralleled by the induction of caspase 3/7 activity and a pronounced increment in oligonucleosomal fragmentation (Fig. 2, *B–D*). The latter was not observed to increase further, most likely because of the release of oligonucleosomes in the culture medium in this apoptosis model. After 6 h of etoposide treatment the level of apoptosis measured in synchronized HeLa cells was similar to that of cells stimulated with TRAIL for 2 h, whereas in the nonsynchronized population a similar degree of nuclear condensation was reached only after 18 h. Cell synchronization thus effectively enhanced the toxicity of etoposide and shifted the onset of the apoptotic response to a time window comparable with that of the TRAIL model. Caspase activity, nuclear condensation, and oligonucleosomal fragmentation were also measured in synchronized cells in the absence of etoposide, revealing that cell synchronization *per se* had no toxic or apoptosis-inducing effect.

Caspase-mediated Cleavage of Only a Few Components of the NPC Core Structure during Apoptosis—Following the induction of apoptosis with either TRAIL or etoposide, we studied the fate of all known NPC components by immunoblot analysis. In both apoptotic models, the same nucleoporins were found to be targets for degradation by caspases (see also supplemental material). Most of these were NPC components that are peripherally attached to the NPC proper, namely RanBP2 and Nup214 at the cytoplasmic side of the NPC and Nup50, Nup153, and Tpr at its nuclear side. In both models, the fragmentation patterns of these nucleoporins were highly similar (Figs. 3 and 4). Cleavage of Nup153 and Tpr yielded major fragments of ~130 and ~190 kDa, respectively, as previously observed in staurosporine and actinomycin D-induced apoptosis (5, 45). RanBP2 degradation resulted in multiple bands migrating between 110 and 250 kDa of molecular mass, whereas

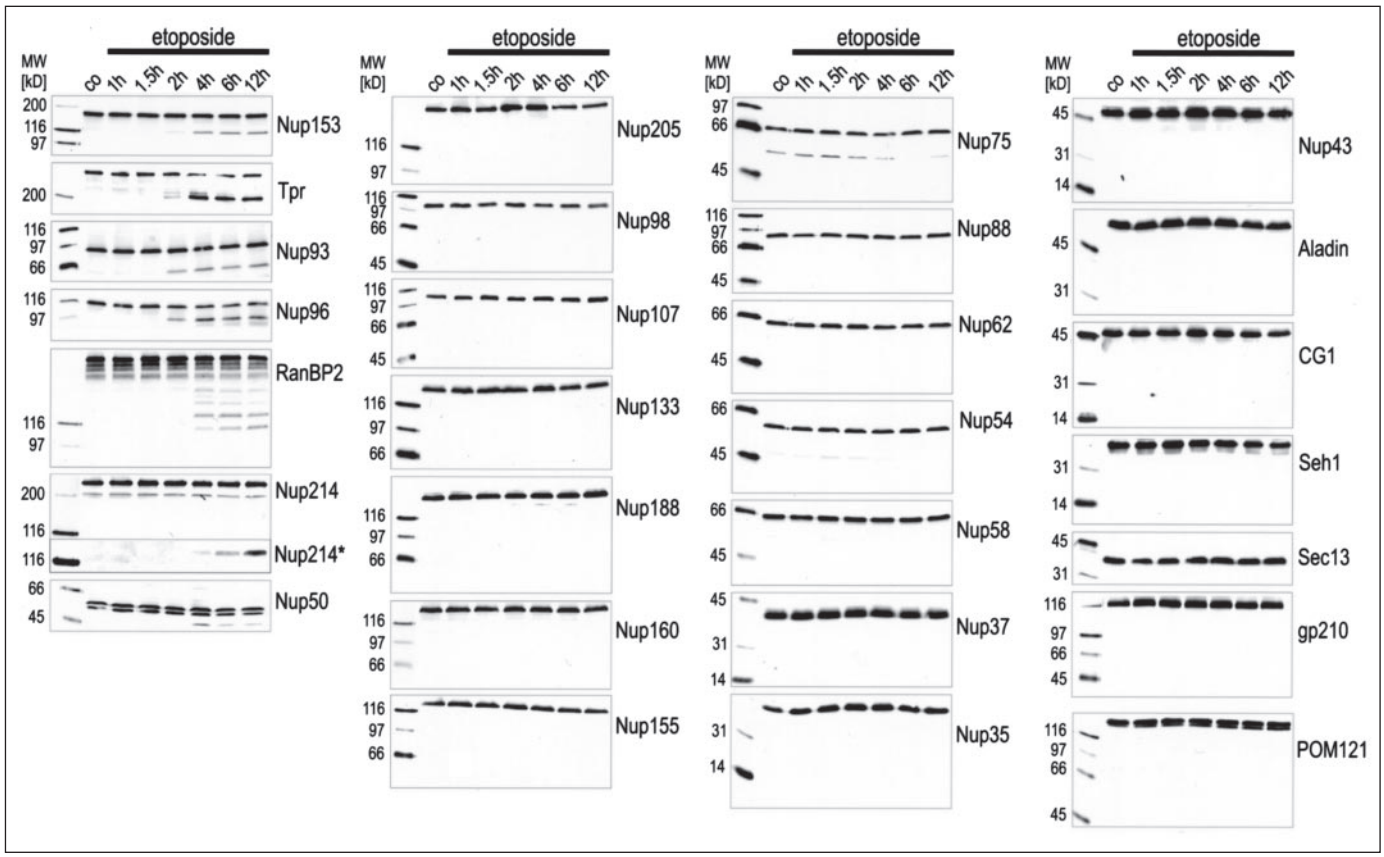

FIGURE 4. **Peripheral nucleoporins and two components of the NPC core structure, Nup93 and Nup96 are cleaved during etoposide-induced apoptosis.** Whole cell extracts were prepared from control (*co*) and apoptotic HeLa cells synchronized in the S phase and treated with 50 μM etoposide. The cells were collected at the indicated time points followed by immunoblot analysis. A long exposure of the Nup214 immunoblot (asterisk) *is* included.

only one proteolytic fragment of ~120 kDa was seen for Nup214, also in line with previous results (5).

Here we also observed apoptotic cleavage of the peripheral NPC component Nup50. Two Nup50 isoforms, *a* and *b*, exist in HeLa cells (60). Isoform *b*, translated from an upstream start codon, is 28 amino acids (aa) longer than isoform *a*, corresponding to a mass difference of 3.3 kDa. Apoptotic cleavage of these Nup50 isoforms yielded a proteolytic product of 48 kDa that was not labeled by an antibody against the N terminus (α-1–21) of isoform *b*, indicating that this part of the protein had been proteolytically removed (Figs. 5*A* and 6).

Whereas apparently most of the peripherally attached nucleoporins are targets for caspases, most of the NPC core components are ignored by these proteases. Of the more than 20 nucleoporins that form the actual NPC core, we found only two, Nup93 and Nup96, that were subjects of caspase-mediated degradation in both TRAIL- and etoposide-induced apoptosis. For Nup93, one cleavage product of ~50 kDa was observed. This fragment was detected with two different antibodies specific for aa 371–389 and 586–606, suggesting that Nup93 is processed at a putative caspase cleavage site located at position 157 ($DALD_{157}$) (Figs. 5*B* and 6). Cleavage of Nup96, a nucleoporin with a molecular mass of 105.9 kDa (12), yielded one major fragment of ~95 kDa and a faint additional band of ~90 kDa. These Nup96 fragments were detected with three different antibodies raised against Nup96 peptides corresponding to aa 130–146, 574–596, and 880–900. These data suggest that the main cleavage sites of Nup96 are also located near the N terminus of the protein, specifically at positions 72 and 124 ($DMVD_{72}$ and $DEED_{124}$) (Figs. 5*B* and 6).

Interestingly, the transmembrane protein Pom121 was among the nucleoporins not cleaved in both apoptotic models. Recently, rat Pom121 has been reported being a substrate for caspase-mediated proteolysis in staurosporine-induced apoptosis of cultured rat and HeLa cells (7, 8). However, in TRAIL- and etoposide-induced apoptosis, no apoptotic fragments of human POM121 were detectable, despite the use of four different antibodies that specifically recognize different Pom121 protein segments (Fig. 5*C*).

Death Receptor-induced Apoptosis and DNA Damage-induced Apoptosis Differ in the Sequence of Cleavage of Peripheral Nucleoporins—The extent and time courses of nucleoporin proteolysis were further assessed by immunoblot signal quantification (Fig. 7). Nup93, Nup96, and RanBP2 were the first nucleoporins that underwent fragmentation upon induction of apoptosis by TRAIL. Such degradation was already noticed 1.5 h after the initial stimulation when ~22% of the cells had undergone apoptosis as judged by morphologic inspection (Fig. 1*A*). Cleavage of Nup153 and Tpr on the nucleoplasmic side became apparent after 2 h (corresponding to an apoptosis level of ~35%). Onset of Nup50 and Nup214 proteolysis was observed even later (3 h). At 3 h post-stimulation, ~40–50% of Nup96, RanBP2, and Tpr were cleaved, in contrast to ~20–30% of Nup50, Nup93, and Nup153.

During DNA damage-induced apoptosis, cleavage of Nup93 and Nup96 was again among the first events to be detected and occurred at 2 h after stimulation with etoposide, when about 11% of the cells displayed an apoptotic morphology (Fig. 1*B*). In this model, proteolysis of the two core nucleoporins occurred concomitantly to that of the nucleoplasmic nucleoporins Nup153 and Tpr. Cleavage products of Nup50, RanBP2, and Nup214 were seen after 4 h. In the absence of etoposide, no nucleoporin cleavage was detectable in synchronized cells (not shown).

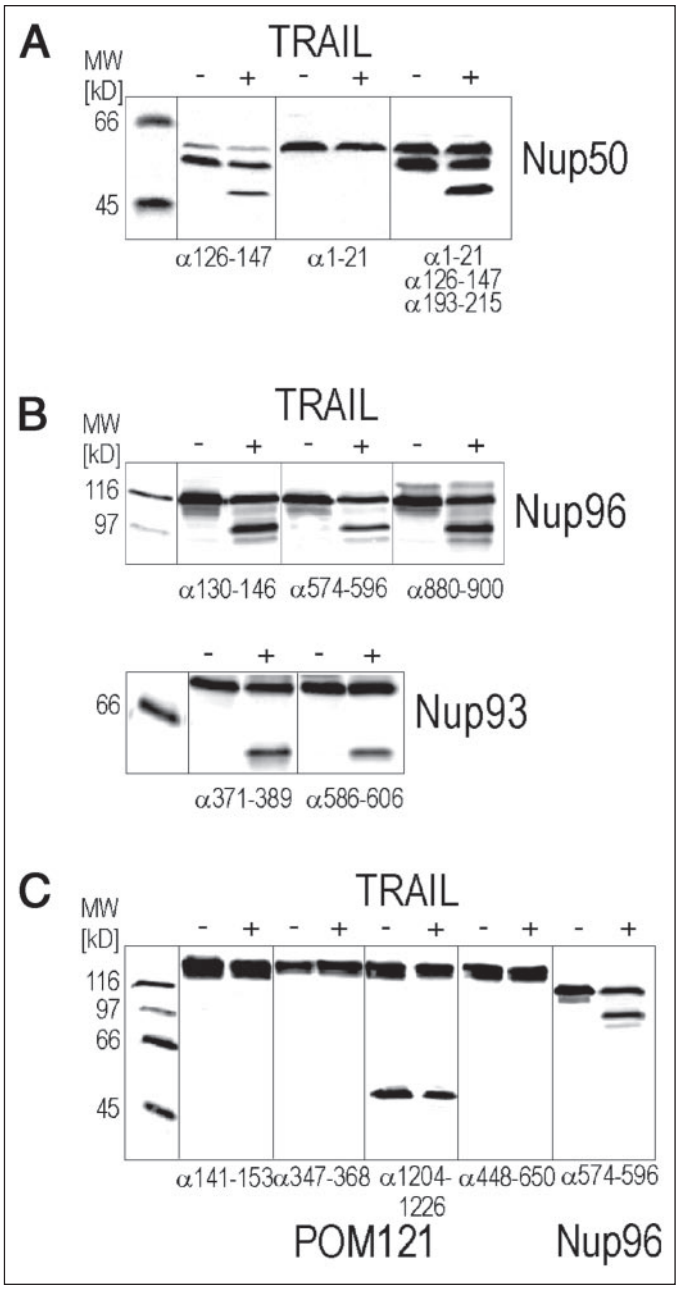

FIGURE 5. **Nup50, Nup93, and Nup96 are processed at sites located near their N termini, whereas POM121 is not cleaved.** *A*, immunoblot analysis of whole cell extracts with Nup50 antibodies against sequence segments comprising aa 126–147, aa 193–215, and the N terminus (aa 1–21) of Nup50 isoform *b*. *B*, immunoblots of whole cell extracts with Nup93 antibodies against sequence segments comprising aa 371–389 and aa 586–606, respectively, and with Nup96 antibodies against aa 130–146, aa 574–596, and aa 880–900. *C*, immunoblots of whole cell extracts with Pom121 antibodies against aa 141–153, aa 347–368, aa 448–650, and aa 1204–1226, respectively. Cleavage of Nup96 in the same cell extract is shown as a control.

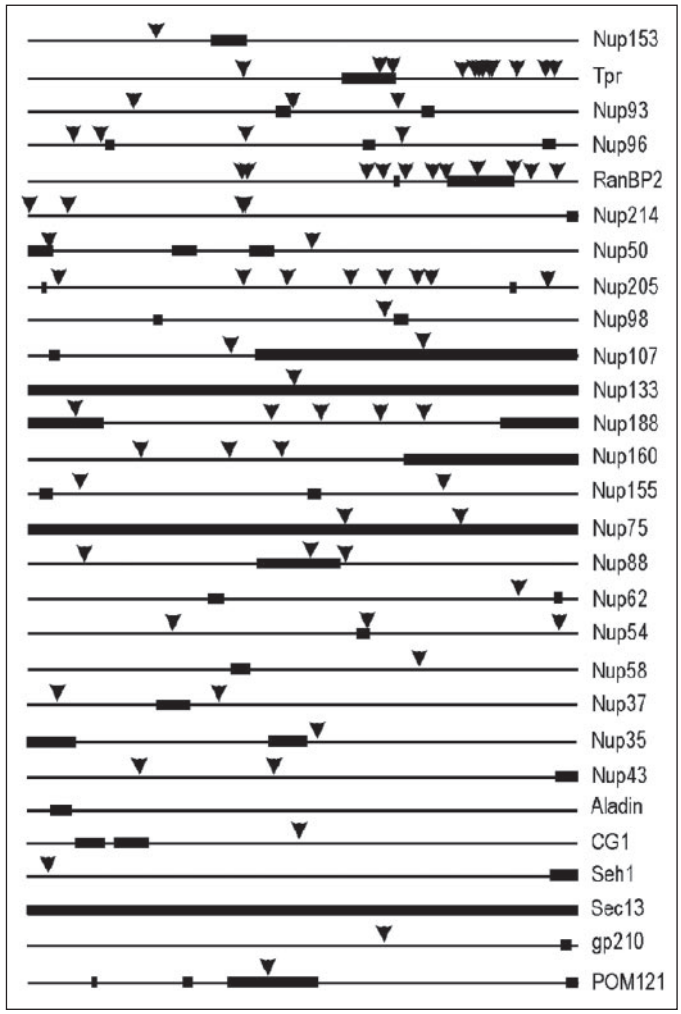

FIGURE 6. **Relative positions of putative caspase cleavage sites and antibody epitopes in the primary structure of nucleoporins.** *Arrowheads* indicate the locations of D*XX*D motifs. *Black boxes* represent the sequence segments used for immunizations, except for Nup153 and Tpr, which were labeled with monoclonal antibodies. Here, *black boxes* demark the regions to which the epitopes recognized by these monoclonal antibodies have been mapped.

Regarding the extent of nucleoporin cleavage, we observed a significantly higher level of proteolytic Tpr products in etoposide-treated cells compared with TRAIL-treated cells (70% *versus* 40% in the late apoptotic populations). Interestingly, RanBP2 cleavage was far less pronounced in etoposide-treated cells than in TRAIL-treated cells (10% *versus* 40%), which might correlate with the cytoplasmic exposure of this nucleoporin. In agreement with previous observations (5), only a minor fraction of Nup214 was processed in both apoptotic models.

Taken together, our data show that only a specific and limited subset of NPC components is cleaved in apoptosis. Depending on their location within the NPC structure, the sequence of cleavage is influenced by the subcellular localization of the initial apoptotic trigger; NPC core components Nup96 and Nup93, symmetrically located on both sides of the NPC midplane, are invariably processed in both apoptotic models at an early time point. The asymmetrically positioned nucleoplasmic Tpr and Nup153 are cleaved concomitantly to Nup96 and Nup93 if the apoptotic trigger is generated in the nucleus but subsequently to them when apoptosis is induced by TRAIL receptor stimulation at the plasma membrane.

Nup93 and Nup96 Are Cleaved Early in TRAIL-induced Apoptosis Independently of Cell Synchronization—To assess whether synchronization of the cells in the S phase may influence caspase-mediated nucleoporin cleavage, we performed immunoblot analysis of Nup153, Tpr, Nup93, Nup96, and RanBP2 in synchronized, TRAIL-treated cells (Fig. 8). Cells in the S phase were generally less sensitive to apoptosis induction by TRAIL. 4 h after treatment less than 40% of these cells displayed an apoptotic morphology as compared with 75% in the nonsynchronized culture (Figs. 1*A* and 8*A*). This observation is consistent with reports on the influence of the cell cycle on TRAIL-dependent cell death (61, 62). Correspondingly, the overall level of nucleoporin cleavage was lower as compared with nonsynchronized cells (Figs. 8, *B* and *C*,

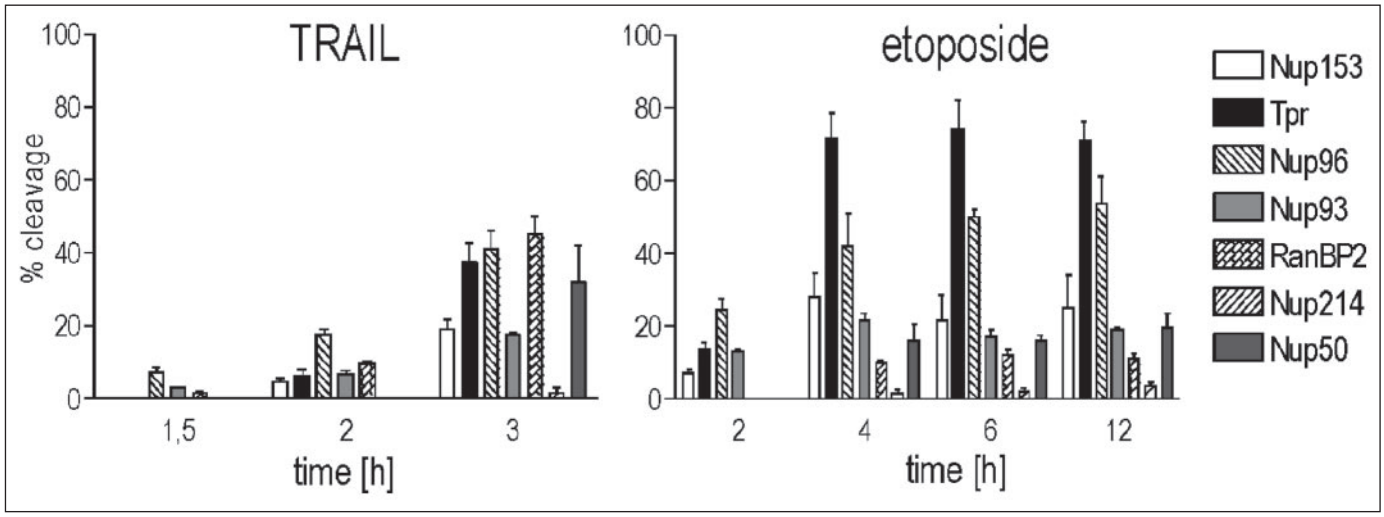

FIGURE 7. **Nup93 and Nup96 are cleaved early during apoptosis.** Chemiluminescent signals from immunoblots for Figs. 3 and 4 were quantified by densitometry. The percentage of cleavage was calculated as the ratio between the signal intensities of the predominant proteolytic product and the intact polypeptide. The data are the means ± standard deviation from at least three separate immunoblots.

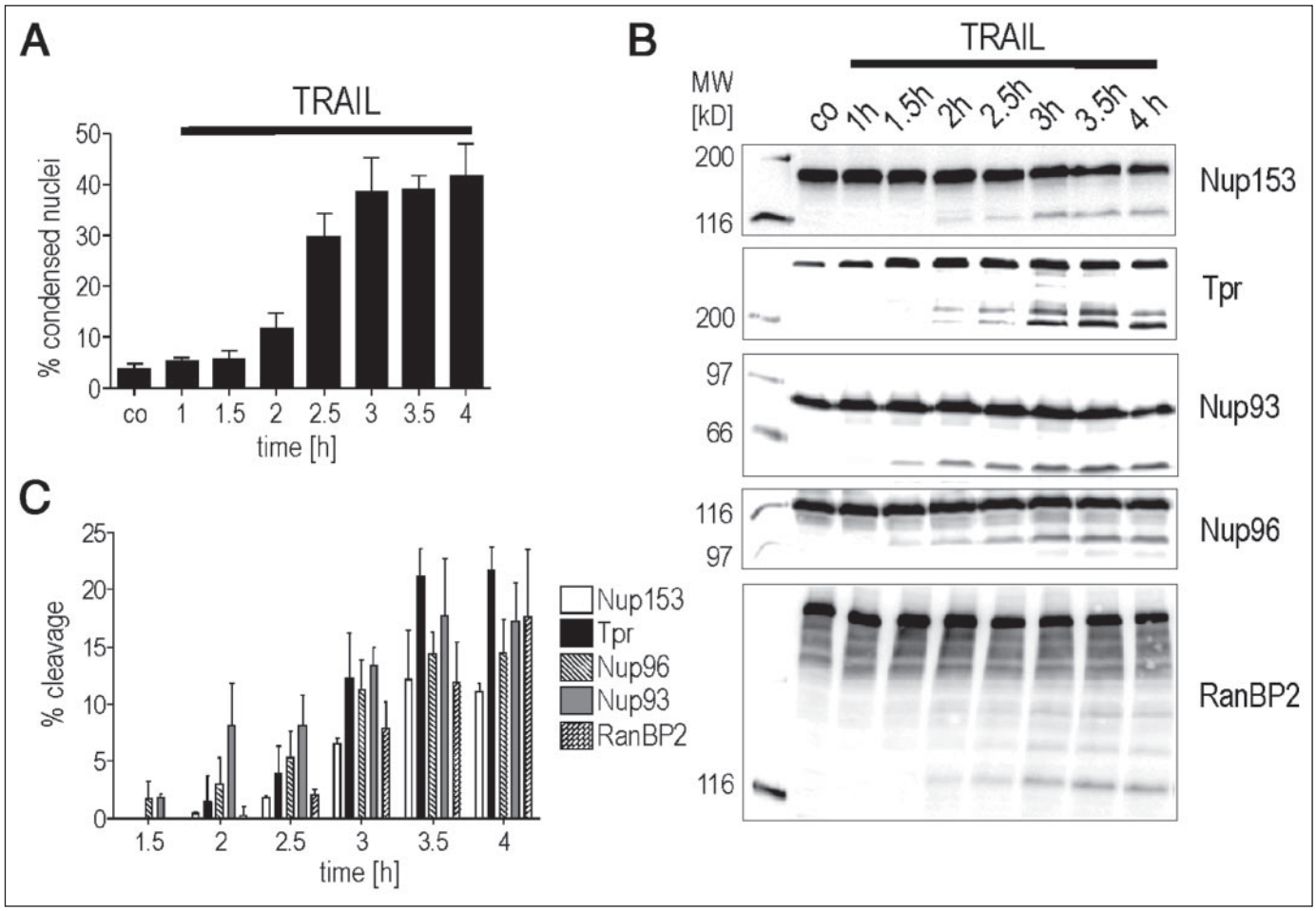

FIGURE 8. **Nup93 and Nup96 are the first NPC components cleaved in synchronized, TRAIL-treated cells.** HeLa cells were synchronized in G_1/S as described in the legend to Fig. 2 and treated with 300 ng/ml TRAIL 4 h after release from the second metabolic block. *A*, at the indicated time points cells were stained with Hoechst 33342 and inspected microscopically. The cells with condensed nuclei were scored as apoptotic. *B*, whole cell extracts were prepared from control (*co*) and apoptotic HeLa cells treated with 300 ng/ml TRAIL after synchronization. The cells were collected at indicated time points, followed by immunoblot analysis with antibodies specific for indicated nucleoporins. *C*, chemiluminescent signals from immunoblots for *B* were quantified by densitometry. The percentage of cleavage was calculated as the ratio between the signal intensities of the predominant proteolytic product and the intact polypeptide. The data are the means ± standard deviation from three separate immunoblots.

and 7). Synchronization, however, highlighted the early timing of Nup93 and Nup96 cleavage, which preceded that of the peripheral nucleoporins and became visible when only 5% of the population had undergone apoptosis at 1.5 h from stimulation (Fig. 8, *A* and *B*). This further corroborates the assumption that Nup93 and Nup96 processing may represent a crucial initiating step in apoptotic NPC demolition.

Cleavage of nucleoplasmic and cytoplasmic nucleoporins appeared concomitantly, at 2 h after treatment (Fig. 8*C*). In TRAIL-induced apoptosis synchronization in the S phase thus seems to predispose the cells to the coordinated processing of the NPC from both the nucleoplasmic and the cytoplasmic side, whereas in etoposide-treated cells, cleavage at the nucleoplasmic side was favored (Fig. 7).

DISCUSSION

Apparently, most nucleoporins peripherally attached to the NPC are favored caspase substrates. These include RanBP2 and Nup214 at the cytoplasmic and Nup153, Tpr, and Nup50 at the nucleoplasmic side of the NPC. RanBP2 and Nup214 have been reported to be important for mRNA export (63) and support tRNA and NES-mediated protein export (33, 64) but to be dispensable for NLS-mediated protein import (30, 65). Tpr appears to be required neither for nuclear protein import and export nor for bulk export of mRNAs (66)[3] but might play a role in quality control of export cargoes (67). Nup153 in turn appears to play a role in the import of a subset of nuclear proteins (38, 68) and in different pathways of protein and mRNA export (69). Nup50 again has been reported to be involved in both nuclear protein import and export (40, 41). Therefore, apoptotic elimination of these asymmetrically positioned nucleoporins while leaving the scaffold structure unaffected might impair certain nucleocytoplasmic transport pathways. However, even the collective absence of all of these peripheral nucleoporins will most likely neither abrogate all active transport across the NPC nor suffice to abolish the function of NPC as a permeability barrier, which is provided by the central core structure of NPC (42, 70).

Within the central framework of the NPC only two nucleoporins, Nup96 and Nup93, were found to be degraded by caspases during apoptosis. This result is in harmony with the observation that the NPC proper still appears morphologically largely intact even in the late stages of apoptosis (45–47). It is also consistent with the prediction that impairment of NPC function during apoptosis (4, 5, 8) might ensue from proteolytic processing at a limited number of strategic sites (7).

Nup96 is most likely processed first at amino acid position 72 and then at position 124. Removal of this short N-terminal segment might still allow the truncated Nup96 protein to remain incorporated within the apoptotic NPC, consistent with its apparent morphological integrity, whereas complete elimination of Nup96 would most likely disintegrate the whole structure, as suggested by RNA interference experiments (12). Most importantly, caspase-mediated proteolysis of the Nup96 N terminus would result in the removal of the binding domain of the protein for Nup98, located within the first 51 amino acids of Nup96 (71). NPCs devoid of Nup98, while retaining a largely intact core structure as shown by electron microscopy, are impaired in certain types of nuclear protein import (72). In addition, Nup98 has been shown to be an essential component of multiple RNA export pathways (73, 74). Apoptotic removal of the docking site for Nup98 at the NPC might therefore disable several nuclear transport pathways. Whether Nup98-deficient NPCs are also less efficient permeability barriers has not been investigated so far.

On the other hand, Nup93, the second NPC core nucleoporin cleaved in apoptosis has been shown in *Caenorhabditis elegans* to be required for maintaining a fully functional permeability barrier (75). Proteolysis of Nup93 by caspases might therefore compromise this aspect of NPC function. Immunoprecipitation and RNA interference experiments have further indicated that Nup93 is involved in anchoring the Nup62 subcomplex to the NPC (10, 12). Apoptotic cleavage of Nup93 at position 157, as suggested by our results, might disrupt the Nup62 binding site on Nup93, which most likely resides within an N-terminal segment of Nup93 and its yeast homolog Nic96 (76, 77). The Nup62 subcomplex and the homologous Nsp1p subcomplex in yeast are believed to play central roles in nucleocytoplasmic transport processes and might contribute to the NPC permeability barrier (42, 78, 79). Destabilized binding of the Nup62 subcomplex to the NPC might therefore affect transport and barrier functions of the NPC simultaneously. On the other hand, electron microscopy of NPCs depleted of Nup62 and other FG repeat nucleoporins revealed a largely normal morphology (79), consistent with the similarly intact appearance of apoptotic NPCs.

Unexpectedly, another NPC core component, Pom121, was not found processed in apoptosis, although the rat homolog had been reported as a caspase target (7, 8). In our study, no caspase-mediated degradation of human Pom121 was observed even at later stages of apoptosis and despite the use of four different antibodies against different Pom121 protein segments. In contrast, when rat Pom121 and especially when YFP-tagged versions of rat Pom121 had been overexpressed in HeLa cells, these were rapidly degraded in apoptosis (7, 8). Apart from sequence differences between human and rat Pom121, these discrepancies might reflect differences in protein folding and NPC binding between the endogenous human and the surplus of recombinant rat Pom121. This in turn might result in the exposure of cleavage sites within the recombinant protein that are not accessible in the wild type.

In the present study we used two well defined inducers of apoptosis that initiate the apoptotic response on opposite sides of the nuclear envelope. Nonetheless, the same nucleoporins were found processed in both model systems, suggesting the existence of an inherent scheme of NPC disablement in apoptotic cells that is independent from the pathway of caspase activation. However, although the selection of caspase targets at the NPC did not vary between the apoptotic models, the sequel of their cleavage was found to differ. A comparison between nonsynchronized and synchronized TRAIL-treated cells revealed that the cell cycle may also influence the temporal sequence of nucleoporin cleavage. This might reflect stimulus-specific differences in the order of activation of individual caspases and their subcellular localization. Further, the observation that during etoposide-induced apoptosis cleavage of Tpr and Nup153 at the nuclear side of the NPC precedes fragmentation of the cytoplasmically oriented nucleoporins suggests the existence of pathways leading to an early activation of caspases in the nucleus.

The parameters that determine why certain nucleoporins are degraded whereas others are not, even though most of them contain consensus sites for caspase cleavage, are presently unclear. Accessibility within the NPC structure might play an important role but is unlikely to be the only determining factor because Nup93, embedded deeply within the NPC core and poorly accessible for antibodies (12), is readily cleaved in apoptotic cells.

In summary, we conclude that apoptotic deactivation of the NPC occurs in a minimalist but most effective manner by surgical targeting of critical sites at seemingly predetermined breaking points, without the necessity of disintegrating the NPC as a whole. Indeed, the individual nucleoporins identified as caspase substrates appear to be components that are dispensable for maintaining the scaffold structure but crucial for different functions of the NPC that need to be terminated during apoptosis.

Acknowledgments—We thank V. Doye, D. Goerlich, W. Hong, R. Kehlenbach, J. Koeser, and F. Melchior for kindly providing antibodies, E. Boneberg and T. Baur for performing FACS analysis, P. Schildknecht for expert technical assistance, and A. Buerkle for critical comments on the manuscript.

[3] V. C. Cordes, unpublished data.

REFERENCES

1. Fuentes-Prior, P., and Salvesen, G. S. (2004) *Biochem. J.* **384,** 201–232
2. Robertson, J. D., Orrenius, S., and Zhivotovsky, B. (2000) *J. Struct. Biol.* **129,** 346–358
3. Earnshaw, W. C. (1995) *Curr. Opin. Cell Biol.* **7,** 337–343
4. Faleiro, L., and Lazebnik, Y. (2000) *J. Cell Biol.* **151,** 951–959
5. Ferrando-May, E., Cordes, V., Biller, I., Görlich, D., Mirkovic, J., and Nicotera, P. (2001) *Cell Death Differ.* **8,** 495–505
6. Roehrig, S., Tabbert, A., and Ferrando-May, E. (2003) *Anal. Biochem.* **318,** 244–253
7. Kihlmark, M., Imreh, G., and Hallberg, E. (2001) *J. Cell Sci.* **114,** 3643–3653
8. Kihlmark, M., Rustum, C., Eriksson, C., Beckman, M., Iverfeldt, K., and Hallberg, E. (2004) *Exp. Cell Res.* **293,** 346–356
9. Cronshaw, J. M., Krutchinsky, A. N., Zhang, W., Chait, B. T., and Matunis, M. J. (2002) *J. Cell Biol.* **158,** 915–927
10. Grandi, P., Dang, T., Panté, N., Shevchenko, A., Mann, M., Forbes, D., and Hurt, E. (1997) *Mol. Biol. Cell* **8,** 2017–2038
11. Miller, B. R., Powers, M., Park, M., Fischer, W., and Forbes, D. J. (2000) *Mol. Biol. Cell* **11,** 3381–3396
12. Krull, S., Thyberg, J., Bjorkroth, B., Rackwitz, H. R., and Cordes, V. C. (2004) *Mol. Biol. Cell* **15,** 4261–4277
13. Finlay, D. R., Meier, E., Bradley, P., Horecka, J., and Forbes, D. J. (1991) *J. Cell Biol.* **114,** 169–183
14. Kita, K., Omata, S., and Horigome, T. (1993) *J. Biochem.* (*Tokyo*) **113,** 377–382
15. Belgareh, N., Rabut, G., Bai, S. W., van Overbeek, M., Beaudouin, J., Daigle, N., Zatsepina, O. V., Pasteau, F., Labas, V., Fromont-Racine, M., Ellenberg, J., and Doye, V. (2001) *J. Cell Biol.* **154,** 1147–1160
16. Vasu, S., Shah, S., Orjalo, A., Park, M., Fischer, W. H., and Forbes, D. J. (2001) *J. Cell Biol.* **155,** 339–354
17. Harel, A., Orjalo, A. V., Vincent, T., Lachish-Zalait, A., Vasu, S., Shah, S., Zimmerman, E., Elbaum, M., and Forbes, D. J. (2003) *Mol. Cell* **11,** 853–864
18. Loiodice, I., Alves, A., Rabut, G., Van Overbeek, M., Ellenberg, J., Sibarita, J. B., and Doye, V. (2004) *Mol. Biol. Cell* **15,** 3333–3344
19. Radu, A., Moore, M. S., and Blobel, G. (1995) *Cell* **81,** 215–222
20. Powers, M. A., Macaulay, C., Masiarz, F. R., and Forbes, D. J. (1995) *J. Cell Biol.* **128,** 721–736
21. Fontoura, B. M., Blobel, G., and Matunis, M. J. (1999) *J. Cell Biol.* **144,** 1097–1112
22. Radu, A., Blobel, G., and Wozniak, R. W. (1993) *J. Cell Biol.* **121,** 1–9
23. Le Rouzic, E., Mousnier, A., Rustum, C., Stutz, F., Hallberg, E., Dargemont, C., and Benichou, S. (2002) *J. Biol. Chem.* **277,** 45091–45098
24. Gerace, L., Ottaviano, Y., and Kondor-Koch, C. (1982) *J. Cell Biol.* **95,** 826–837
25. Wozniak, R. W., Bartnik, E., and Blobel, G. (1989) *J. Cell Biol.* **108,** 2083–2092
26. Hallberg, E., Wozniak, R. W., and Blobel, G. (1993) *J. Cell Biol.* **122,** 513–521
27. Wu, J., Matunis, M. J., Kraemer, D., Blobel, G., and Coutavas, E. (1995) *J. Biol. Chem.* **270,** 14209–14213
28. Yokoyama, N., Hayashi, N., Seki, T., Pante, N., Ohba, T., Nishii, K., Kuma, K., Hayashida, T., Miyata, T., Aebi, U., Fukui, M., and Nishimoto, T. (1995) *Nature* **376,** 184–188
29. Kraemer, D., Wozniak, R. W., Blobel, G., and Radu, A. (1994) *Proc. Natl. Acad. Sci. U. S. A.* **91,** 1519–1523
30. Walther, T. C., Pickersgill, H. S., Cordes, V. C., Goldberg, M. W., Allen, T. D., Mattaj, I. W., and Fornerod, M. (2002) *J. Cell Biol.* **158,** 63–77
31. Fornerod, M., van Deursen, J., van Baal, S., Reynolds, A., Davis, D., Murti, K. G., Fransen, J., and Grosveld, G. (1997) *EMBO J.* **16,** 807–816
32. Bastos, R., Ribas de Pouplana, L., Enarson, M., Bodoor, K., and Burke, B. (1997) *J. Cell Biol.* **137,** 989–1000
33. Bernad, R., van der Velde, H., Fornerod, M., and Pickersgill, H. (2004) *Mol. Cell. Biol.* **24,** 2373–2384
34. Ris, H. (1991) *EMSA Bull.* **21,** 54–56
35. Jarnik, M., and Aebi, U. (1991) *J. Struct. Biol.* **107,** 291–308
36. Cordes, V. C., Reidenbach, S., Rackwitz, H.-R., and Franke, W. W. (1997) *J. Cell Biol.* **136,** 515–529
37. Sukegawa, J., and Blobel, G. (1993) *Cell* **72,** 29–38
38. Walther, T. C., Fornerod, M., Pickersgill, H., Goldberg, M., Allen, T. D., and Mattaj, I. W. (2001) *EMBO J.* **20,** 5703–5714
39. Hase, M. E., and Cordes, V. C. (2003) *Mol. Biol. Cell* **14,** 1923–1940
40. Guan, T., Kehlenbach, R. H., Schirmer, E. C., Kehlenbach, A., Fan, F., Clurman, B. E., Arnheim, N., and Gerace, L. (2000) *Mol. Cell. Biol.* **20,** 5619–5630
41. Lindsay, M. E., Plafker, K., Smith, A. E., Clurman, B. E., and Macara, I. G. (2002) *Cell* **110,** 349–360
42. Strawn, L. A., Shen, T., Shulga, N., Goldfarb, D. S., and Wente, S. R. (2004) *Nat. Cell Biol.* **6,** 197–206
43. Fried, H., and Kutay, U. (2003) *Cell Mol. Life Sci.* **60,** 1659–1688
44. Ribbeck, K., and Gorlich, D. (2001) *EMBO J.* **20,** 1320–1330
45. Buendia, B., Santa-Maria, A., and Courvalin, J. C. (1999) *J. Cell Sci.* **112,** 1743–1753
46. Lazebnik, Y. A., Cole, S., Cooke, C. A., Nelson, W. G., and Earnshaw, W. C. (1993) *J. Cell Biol.* **123,** 7–22
47. Falcieri, E., Gobbi, P., Cataldi, A., Zamai, L., Faenza, I., and Vitale, M. (1994) *Histochem. J.* **26,** 754–763
48. Wiley, S. R., Schooley, K., Smolak, P. J., Din, W. S., Huang, C. P., Nicholl, J. K., Sutherland, G. R., Smith, T. D., Rauch, C., Smith, C. A., and Goodwin, R. G. (1995) *Immunity* **3,** 673–682
49. Walczak, H., Degli-Esposti, M. A., Johnson, R. S., Smolak, P. J., Waugh, J. Y., Boiani, N., Timour, M. S., Gerhart, M. J., Schooley, K. A., Smith, C. A., Goodwin, R. G., and Rauch, C. T. (1997) *EMBO J.* **16,** 5386–5397
50. Froelich-Ammon, S. J., and Osheroff, N. (1995) *J. Biol. Chem.* **270,** 21429–21432
51. Walczak, H., Miller, R. E., Ariail, K., Gliniak, B., Griffith, T. S., Kubin, M., Chin, W., Jones, J., Woodward, A., Le, T., Smith, C., Smolak, P., Goodwin, R. G., Rauch, C. T., Schuh, J. C., and Lynch, D. H. (1999) *Nat. Med.* **5,** 157–163
52. Thornberry, N. A. (1994) *Methods Enzymol.* **244,** 615–631
53. Leist, M., Volbracht, C., Kuhnle, S., Fava, E., Ferrando-May, E., and Nicotera, P. (1997) *Mol. Med.* **3,** 750–764
54. Thomas, J. O., and Kornberg, R. D. (1975) *Proc. Natl. Acad. Sci. U. S. A.* **72,** 2626–2630
55. Cordes, V. C., Reidenbach, S., Köhler, A., Stuurman, N., van Driel, R., and Franke, W. W. (1993) *J. Cell Biol.* **123,** 1333–1344
56. Cordes, V. C., Waizenegger, I., and Krohne, G. (1991) *Eur. J. Cell Biol.* **55,** 31–47
57. Karpinich, N. O., Tafani, M., Rothman, R. J., Russo, M. A., and Farber, J. L. (2002) *J. Biol. Chem.* **277,** 16547–16552
58. Yim, H., Jin, Y. H., Park, B. D., Choi, H. J., and Lee, S. K. (2003) *Mol. Biol. Cell* **14,** 4250–4259
59. Chow, K. C., and Ross, W. E. (1987) *Mol. Cell. Biol.* **7,** 3119–3123
60. Trichet, V., Shkolny, D., Dunham, I., Beare, D., and McDermid, H. E. (1999) *Cytogenet. Cell Genet.* **85,** 221–226
61. Jin, Z., Dicker, D. T., and El-Deiry, W. S. (2002) *Cell Cycle* **1,** 82–89
62. Lu, M., Kwan, T., Yu, C., Chen, F., Freedman, B., Schafer, J. M., Lee, E. J., Jameson, J. L., Jordan, V. C., and Cryns, V. L. (2005) *J. Biol. Chem.* **280,** 6742–6751
63. Forler, D., Rabut, G., Ciccarelli, F. D., Herold, A., Kocher, T., Niggeweg, R., Bork, P., Ellenberg, J., and Izaurralde, E. (2004) *Mol. Cell. Biol.* **24,** 1155–1167
64. Kuersten, S., Arts, G. J., Walther, T. C., Englmeier, L., and Mattaj, I. W. (2002) *Mol. Cell. Biol.* **22,** 5708–5720
65. van Deursen, J., Boer, J., Kasper, L., and Grosveld, G. (1996) *EMBO J.* **15,** 5574–5583
66. Shibata, S., Matsuoka, Y., and Yoneda, Y. (2002) *Genes Cells* **7,** 421–434
67. Galy, V., Gadal, O., Fromont-Racine, M., Romano, A., Jacquier, A., and Nehrbass, U. (2004) *Cell* **116,** 63–73
68. Shah, S., and Forbes, D. J. (1998) *Curr. Biol.* **8,** 1376–1386
69. Ullman, K. S., Shah, S., Powers, M. A., and Forbes, D. J. (1999) *Mol. Biol. Cell* **10,** 649–664
70. Zeitler, B., and Weis, K. (2004) *J. Cell Biol.* **167,** 583–590
71. Rosenblum, J. S., and Blobel, G. (1999) *Proc. Natl. Acad. Sci. U. S. A.* **96,** 11370–11375
72. Wu, X., Kasper, L. H., Mantcheva, R. T., Mantchev, G. T., Springett, M. J., and van Deursen, J. M. (2001) *Proc. Natl. Acad. Sci. U. S. A.* **98,** 3191–3196
73. Powers, M. A., Forbes, D. J., Dahlberg, J. E., and Lund, E. (1997) *J. Cell Biol.* **136,** 241–250
74. Pritchard, C. E., Fornerod, M., Kasper, L. H., and van Deursen, J. M. (1999) *J. Cell Biol.* **145,** 237–254
75. Galy, V., Mattaj, I. W., and Askjaer, P. (2003) *Mol. Biol. Cell* **14,** 5104–5115
76. Grandi, P., Schlaich, N., Tekotte, H., and Hurt, E. C. (1995) *EMBO J.* **14,** 76–87
77. Schlaich, N. L., Häner, M., Lustig, A., Aebi, U., and Hurt, E. C. (1997) *Mol. Biol. Cell* **8,** 33–46
78. Denning, D. P., Patel, S. S., Uversky, V., Fink, A. L., and Rexach, M. (2003) *Proc. Natl. Acad. Sci. U. S. A.* **100,** 2450–2455
79. Finlay, D. R., and Forbes, D. J. (1990) *Cell* **60,** 17–29

Protein Synthesis, Post-Translation Modification, and Degradation:

Caspases Target Only Two Architectural Components within the Core Structure of the Nuclear Pore Complex

Monika Patre, Anja Tabbert, Daniela Hermann, Henning Walczak, Hans-Richard Rackwitz, Volker C. Cordes and Elisa Ferrando-May

J. Biol. Chem. 2006, 281:1296-1304.
doi: 10.1074/jbc.M511717200 originally published online November 14, 2005